






ORIGINAL ARTICLE

Mast cells selectively target large cholangiocytes during biliary injury via H2HR-mediated cAMP/pERK1/2 signaling

Tianhao Zhou¹ | Vik Meadows¹ | Debjyoti Kundu¹ | Konstantina Kyritsi¹ |
 Travis Owen¹ | Ludovica Ceci¹ | Guido Carpino²  | Paolo Onori³ |
 Eugenio Gaudio³ | Nan Wu¹ | Shannon Glaser⁴ | Burcin Ekser⁵  |
 Gianfranco Alpini^{1,6}  | Lindsey Kennedy^{1,6}  | Heather Francis^{1,6} 

¹Division of Gastroenterology and Hepatology, Department of Medicine, Indiana University School of Medicine Research, Indianapolis, Indiana, USA

²Department of Movement, Human and Health Sciences, University of Rome "Foro Italico", Rome, Italy

³Department of Anatomical, Histological, Forensic Medicine and Orthopedics Sciences, Sapienza University of Rome, Rome, Italy

⁴Department of Medical Physiology, Texas A&M University, Bryan, Texas, USA

⁵Division of Transplant Surgery, Department of Surgery, Indiana University School of Medicine, Indianapolis, Indiana, USA

⁶Richard L. Roudebush VA Medical Center, Indianapolis, Indiana, USA

Correspondence

Lindsey Kennedy, Assistant Research Professor, VA Health Science Specialist, Indiana University School of Medicine, Gastroenterology and Hepatology, Richard L. Roudebush VA Medical Center, Department of Research, 702 Rotary Circle, Room 007, Indianapolis, IN 46202, USA.

Email: linkenn@iu.edu

Heather Francis, VA Research Career Scientist, Indiana Center for Liver Research, Richard L. Roudebush VA Medical Center and Indiana University, Gastroenterology, Medicine, 702 Rotary Circle, 013C, Indianapolis, IN 46202, USA.

Email: heafranc@iu.edu

Funding information

National Institute of Diabetes and Digestive and Kidney Diseases, Grant/Award Number: DK054811, DK062975, DK076898, DK107310, DK108959, DK110035, DK115184 and DK119421; National Institute on Alcohol Abuse and Alcoholism, Grant/Award Number: AA028711; U.S. Department of Veterans Affairs, Grant/Award Number: 11K2BX005306, 5I01BX000574, 5I01BX003031, IK6 BX004601 and IK6BX005226

Abstract

Bile ducts are heterogeneous in structure and function, and primary sclerosing cholangitis (PSC) damages specific bile ducts leading to ductular reaction (DR), mast cell (MC) infiltration, increased histamine release, inflammation, and fibrosis. Bile duct ligation (BDL) induces large duct damage via cyclic adenosine monophosphate (cAMP)/extracellular signal-related protein kinase (ERK) signaling, and large cholangiocytes express H2 histamine receptor (H2HR). We evaluated how MCs interact with large cholangiocytes during cholestasis. Male wild-type (WT) and MC-deficient (*Kit^{W^{-sh}}*) mice 10–12 weeks of age were subjected to BDL for 7 days. Select *Kit^{W^{-sh}}* mice were injected with MCs pretreated with control or H2HR antagonist (ranitidine, 25 μm, 48 h) via tail vein injection. *In vitro*, MC migration toward small mouse cholangiocytes (SMCCs) and large mouse cholangiocytes (LMCCs) treated with lipopolysaccharide or histamine (±ranitidine) was measured. LMCCs were stimulated with MC supernatants pretreated with control, α-methyl-dl-histidine (to block histamine release), or ranitidine. Liver damage, large duct DR/senescence, inflammation, fibrosis, and cAMP/ERK immunoreactivity increased in BDL WT and *Kit^{W^{-sh}}*+MC mice but decreased in BDL *Kit^{W^{-sh}}* and *Kit^{W^{-sh}}*+MC-H2HR mice. *In vitro*, MCs migrate toward damaged LMCCs (but not SMCCs) blocked by inhibition of H2HR. Loss of MC histamine or

Tianhao Zhou and Vik Meadows sharing first authorship.

This is an open access article under the terms of the [Creative Commons Attribution-NonCommercial-NoDerivs](https://creativecommons.org/licenses/by-nc-nd/4.0/) License, which permits use and distribution in any medium, provided the original work is properly cited, the use is non-commercial and no modifications or adaptations are made.

© 2022 The Authors. *Hepatology Communications* published by Wiley Periodicals LLC on behalf of American Association for the Study of Liver Diseases.

MC-H2HR decreases LMCC proliferation, senescence, H2HR, and cAMP/ERK levels. Human PSC livers have increased MC number found near DR, senescent ducts, and H2HR-positive ducts. **Conclusion:** Infiltrating MCs preferentially interact with large ducts via H2HR signaling promoting biliary and liver damage. Mediation of MCs may be a therapeutic strategy for PSC.

INTRODUCTION

Cholangiopathies target different subpopulations of small and large cholangiocytes, and the biliary tree is morphologically, phenotypically, and functionally heterogeneous; however, there are specific differences between species.^[1–3] The heterogeneous phenotypes of the biliary epithelium have been established by *ex situ* morphology and *in vitro* in cholangiocytes isolated from normal and liver injury models.^[4] Small bile ducts are lined by small cholangiocytes and large bile ducts are surrounded by large cholangiocytes.^[1–3] Small cholangiocytes are cuboidal and respond to injury via inositol 1,4,5-triphosphate/calcium (Ca²⁺) signaling, whereas large cholangiocytes are more columnar in shape and signal through cyclic adenosine monophosphate/extracellular regulated kinase 1/2 (cAMP/ERK1/2) mechanisms.^[4–6] Following specific damage such as carbon tetrachloride or gamma-aminobutyric acid treatment, large cholangiocytes become injured, and small cholangiocytes *de novo* proliferate assuming large biliary phenotypes.^[7–9] Large bile ducts are the primary target of primary sclerosing cholangitis (PSC). Patients with classical PSC (encompassing large duct damage) comprise about 90% of diagnoses and are more at risk to develop cholangiocarcinoma (CCA).^[10]

Histamine (HA) interacts with four G protein-coupled receptors, H1-H4 HA receptors (HRs), and it has been demonstrated that H1 histamine receptor (H1HR) binds to G_{α_i}, inducing Ca²⁺-mediated intracellular signaling. In contrast, H2 histamine receptor (H2HR) preferentially binds to G_{α_s}, activating the cAMP/ERK pathway.^[11,12] Mast cells (MCs) are a prime source of HA, and both MCs and HA levels are exacerbated during cholestatic liver injury, as demonstrated in animal models and human cholestatic diseases.^[13] Patients with PSC have higher biliary expression of H1HR and H2HR, and inhibition of either or both receptors decreases PSC phenotypes in multidrug resistant 2 knockout (*Mdr2*^{-/-}) mice and reduces tumor growth and CCA-induced angiogenesis in xenograft models.^[14] Both cholangiocytes and MCs (found in nearby bile ducts) express HRs, which induce paracrine crosstalk during liver injury, contributing to disease progression.^[12,13]

In mice lacking MCs (*Kit*^{W^{-sh}}) subjected to bile duct ligation (BDL, cholestatic model), large ductal mass and hepatic fibrosis decreased compared with wild-type

(WT) BDL mice.^[15] *Kit*^{W^{-sh}} mice treated with a single tail vein injection (TVI) of cultured MCs have induced biliary damage, inflammation, and hepatic fibrosis,^[15] demonstrating that MCs contribute to cholestatic injury. Since MCs migrate to the liver following injury, and reside in close proximity to bile ducts,^[14–16] there is a high probability that damaged/proliferating cholangiocytes induce MC migration. Inhibition of biliary stem cell factor (SCF) by Vivo Morpholino treatment blocks MC recruitment to the portal tract of *Mdr2*^{-/-} mice, resulting in amelioration of PSC phenotypes.^[17] Furthermore, increased biliary senescence results in elevated senescence-associated secretory phenotypes (SASPs), which induce MC migration since most SASP factors are also chemoattractants for MCs.^[17,18]

Inhibition of biliary H2HR via Vivo Morpholino treatment targets large duct damage and ameliorates hepatic inflammation and fibrosis^[19]; however, we did not define the role of MCs or MC-H2HR on large duct phenotypes in models of cholestasis. Although the role of MCs in the regulation of cholestasis has been broadly studied, no evidence has addressed the specific role that MCs have on small and large cholangiocytes or if there is a preference for these subpopulations during liver damage.

MATERIALS AND METHODS

Reagents and materials

Reagents for cell culture were obtained from Invitrogen Corp. Total RNA was isolated from total liver and cultured cells using the TRI Reagent from Sigma Life Science and was reverse-transcribed with the Reaction Ready First Strand cDNA Synthesis kit (Qiagen). For staining in mouse sections, formalin-fixed paraffin-embedded, and optimal cutting temperature (OCT)-embedded samples were sectioned at 4–6 μm, and 10 fields were analyzed from 4–8 mice per group. List of primers used is given in Table S1 and antibodies used are found in Table S2.

Animal models

Male C57BL6/J (WT) and MC-deficient C57BL/6J-*Kit*^{W^{-sh}}/J (*Kit*^{W^{-sh}}) mice were obtained from Jackson

Laboratory and were subjected to BDL surgery at 12 weeks of age up to 7 days as described.^[15] Additionally, selected *Kit^{W-sh}* mice received one TVI with sterile, cultured MCs (MC/9 [ATCC], 5×10^6 cells) or $1 \times$ phosphate buffered saline (PBS, control, 0.1 ml) 3 days before sacrifice.^[15,18] Before injection, MCs were tagged with PKH26 Red Fluorescent Linker, and we have previously shown efficient delivery to the liver following TVI of MCs.^[15,18] To determine whether MC-H2HR plays a role in large ductal damage, a subset of *Kit^{W-sh}* mice were injected with MCs pretreated with the H2HR inhibitor, ranitidine ($25 \mu\text{m}$)^[14] for up to 48 h before injection. A minimum of 4–8 mice were used per group. Animals were housed in micro-isolator cages in a temperature-controlled environment with 12/12-h light/dark cycles and were fed *ad libitum* standard chow with free access to drinking water. Liver tissue for snap-frozen samples, OCT-embedded blocks, and formalin-fixed paraffin-embedded blocks, and serum, cholangiocytes and cholangiocyte supernatants, were collected.^[17,18] Animal procedures were performed according to protocols approved by the Baylor Scott and White Health and Indiana University–Purdue University Indianapolis Institutional Animal Care and Use Committees, at Temple, Texas, and Indianapolis, Indiana, respectively.

Human samples

Human liver tissues were collected from patients diagnosed with late-stage PSC (or from control livers) by Dr. Burcin Ekser at Indiana University School of Medicine, and additional controls were purchased from Sekisui XenoTech, LLC. Explant tissues were obtained from transplant, and the diagnosis of PSC was determined by clinical, imaging, and pathological analyses. Written, informed consent was obtained from each patient and reflected in a prior approval by the Indiana University internal review board, and all studies were bound by the Ethical Principles for Medical Research Involving Human Subjects outlined in the 2013 Declaration of Helsinki. Samples were deidentified, and patient information is provided in Table S3.

MC infiltration and H2HR expression

MC infiltration was determined by staining for tryptase beta 2 (Tps β 2) in WT and BDL WT mice along with semi-quantification by counting Tps β 2-positive cells from three to five different portal areas per mouse. Similarly, MC infiltration in human control and PSC samples were imaged by tryptase staining and semi-quantification by counting the number of positively stained cells from five different portal areas per sample. WT and BDL WT mice, as well as control and human PSC livers, were

stained for MCs (Tps β 2 and tryptase, respectively) and cytokeratin 19 (CK-19) to determine MC localization to peribiliary regions. In WT and BDL WT mice, biliary expression of H2HR was evaluated by immunohistochemistry and immunofluorescence co-stained with CK-19. Human control and PSC livers were stained for H2HR/tryptase to evaluate MC localization with H2HR-positive ducts along with semi-quantification of H2HR-positive cholangiocytes from five different portal areas per sample using ImagePro 10 Software (Media Cybernetics Inc.).

Effects of H2HR on MC activation, *in vitro*, and confirmation of injected MC localization, *in vivo*

Prior to injection into *Kit^{W-sh}* mice, MCs were treated with ranitidine, and we confirmed that inhibition of H2HR decreased activation by measuring MC markers (chymase, FC epsilon receptor 1 subunits, FC ϵ R1 α and FC ϵ R1 γ) by quantitative real-time polymerase chain reaction (PCR) and MC HA secretion by EIA (Cayman Chemical).^[15,18] To confirm that injected MCs migrate to the liver and reside close by bile ducts, we performed immunofluorescent staining for CK-19 in the livers from *Kit^{W-sh}* mice injected with control MCs and verified hepatic location of injected MCs using confocal microscopy to image PKH26-tagged MCs.^[15,18] Semi-quantification of MC localization and CK-19-positive bile ducts was performed in two to three representative images ($\times 20$) per mouse from $n = 5$ –6 mice/group using ImagePro 10 Software; each data point represents the average positive area of one mouse.

Liver damage, small and large intrahepatic bile duct mass and biliary senescence

Hematoxylin and eosin staining was performed on all groups of mice, and large ductal damage, necrotic areas, and inflammation were evaluated and scored. CK-19 immunohistochemistry was performed and small and large intrahepatic bile duct mass (IBDM) assessed using ImagePro 10 Software. Small and large IBDM was calculated by the total area of small or large ducts in an image over the total area $\times 100$ (shown as percentage). Differences between small and large bile ducts was determined by luminal size, with small ducts being $< 15 \mu\text{m}$ diameter and large ducts measuring $\geq 15 \mu\text{m}$ diameter.^[4]

We evaluated cholangiocyte senescence by immunofluorescence for cyclin-dependent kinase inhibitor 2A (p16) co-stained with CK-19 along with semi-quantification performed in two to three representative images ($\times 20$) per mouse from $n = 4$ –6 mice/group using ImagePro 10 Software; each data point

represents the average positive area of one mouse. Human control and PSC livers were stained for p16/tryptase to determine MC localization and biliary senescence; semi-quantification was performed for the number of p16-positive cholangiocytes and tryptase-positive MCs within the portal areas as stated previously.

Hepatic fibrosis, hepatic stellate cell activation, inflammation, and intracellular signaling

Hepatic fibrosis was determined by fast green/sirius red (FG/SR) staining with semi-quantification using ImagePro 10 Software and Masson's trichrome staining.^[15] WT and BDL WT mice and human control and PSC samples were stained for CK-19 and FG/SR to demonstrate congruence of hepatic fibrosis with large bile ducts. In WT and BDL WT mice along with human control and PSC samples, we performed staining for FG/SR coupled with either Tps β 2 or tryptase, respectively, to associate hepatic fibrosis with MC presence. Hepatic stellate cell (HSC) activation was determined by immunofluorescence for desmin (co-stained with CK-19) and glial fibrillary acidic protein (GFAP). GFAP immunoreactivity was semi-quantified in two to three representative images ($\times 10$) per mouse from $n = 4-6$ mice/group using ImagePro 10 Software; each data point represents the average positive area of one mouse.

Hepatic inflammation was determined by staining for F4/80 (Kupffer cell marker) along with semi-quantification using ImagePro 10 Software and quantitative PCR for the inflammatory chemokine, C-C motif chemokine ligand 2 (CCL-2), in total liver messenger RNA.

Activation of H2HR increases large cholangiocyte proliferation by cAMP-mediated ERK1/2 phosphorylation.^[5,6] Downstream immunoreactivity of cAMP and ERK was determined by immunofluorescence co-stained with CK-19 along with semi-quantification performed in two to three representative images ($\times 20$) per mouse from $n = 4-6$ mice/group using ImagePro 10 Software; each data point represents the average positive area of one mouse.

In vitro cell line characterization

For *in vitro* experiments we used immortalized, cultured murine small mouse and large mouse cholangiocyte (SMCC and LMCC, respectively) cell lines, which display phenotypes similar to freshly isolated small and large cholangiocytes,^[6] and the murine hepatic MC cell line (MC/9, ATCC) that expresses H1/H2 HRs.^[14] We characterized the immortalized SMCCs and LMCCs

using immunofluorescence for CK-19, H2HR, and senescence (p16 and p18) along with determining cell size using a Countess II FL Automated Cell Counter (Thermo Fisher Scientific).

In vitro MC migration assay

SMCCs and LMCCs were placed in the bottom well of Boyden chambers and pretreated with lipopolysaccharide (LPS, 100 ng/ml) or control (distilled water) for 24 h. Treated SMCCs and LMCCs were washed and replaced with fresh media, and then the top well of the Boyden chambers was filled with MCs to allow for migration through the Transwell membrane for 24 h. MCs were imaged by Toluidine blue staining and quantified by counting of 10 fields per treatment.^[17] In separate experiments, LMCCs were placed in the lower chamber and pretreated with ranitidine (25 μ m) for 30 min before being stimulated with HA (10 μ m) for 24 h. LMCCs were washed and replaced with fresh media, and MCs were placed in the upper chamber and migration measured after 24 h.

Effects of MC-derived HA and inhibition of MC-H2HR on SMCC and LMCC phenotypes, *in vitro*

In vitro, SMCCs and LMCCs were treated with 100 μ l of supernatant from partially activated cultured MCs (T-STIM treatment) or no treatment (control) for 24 h. Treated SMCCs and LMCCs were evaluated for senescence by (i) quantitative PCR for p16 and p18 and (ii) p18 immunofluorescence. Cultured MCs (partially activated by T-STIM) were treated with a global l-histidine decarboxylase (HDC) inhibitor, α -methyl-dl-histidine (α -Me, 3 mM) for 24 h; treated MC supernatants were then placed on LMCC as described previously, and these cells were evaluated by immunofluorescent staining for (i) p18, (ii) H2HR, and (iii) pERK1/2 expression. Finally, LMCCs were treated with control or media from MCs pretreated with vehicle or ranitidine as described and evaluated for senescence (p16 and p18), H2HR, and ERK1/2 expression by immunofluorescence, and cAMP activity in isolated cAMP samples using the Cyclic AMP ELISA Kit (Cayman Chemical).

Statistical analysis

Data are presented as mean \pm SEM. Student's unpaired t-test was used when two groups were analyzed. When more than two groups were analyzed, one-way analysis of variance with Tukey's multiple comparisons test was used with GraphPad Prism 9. We considered $p < 0.05$ as significant.

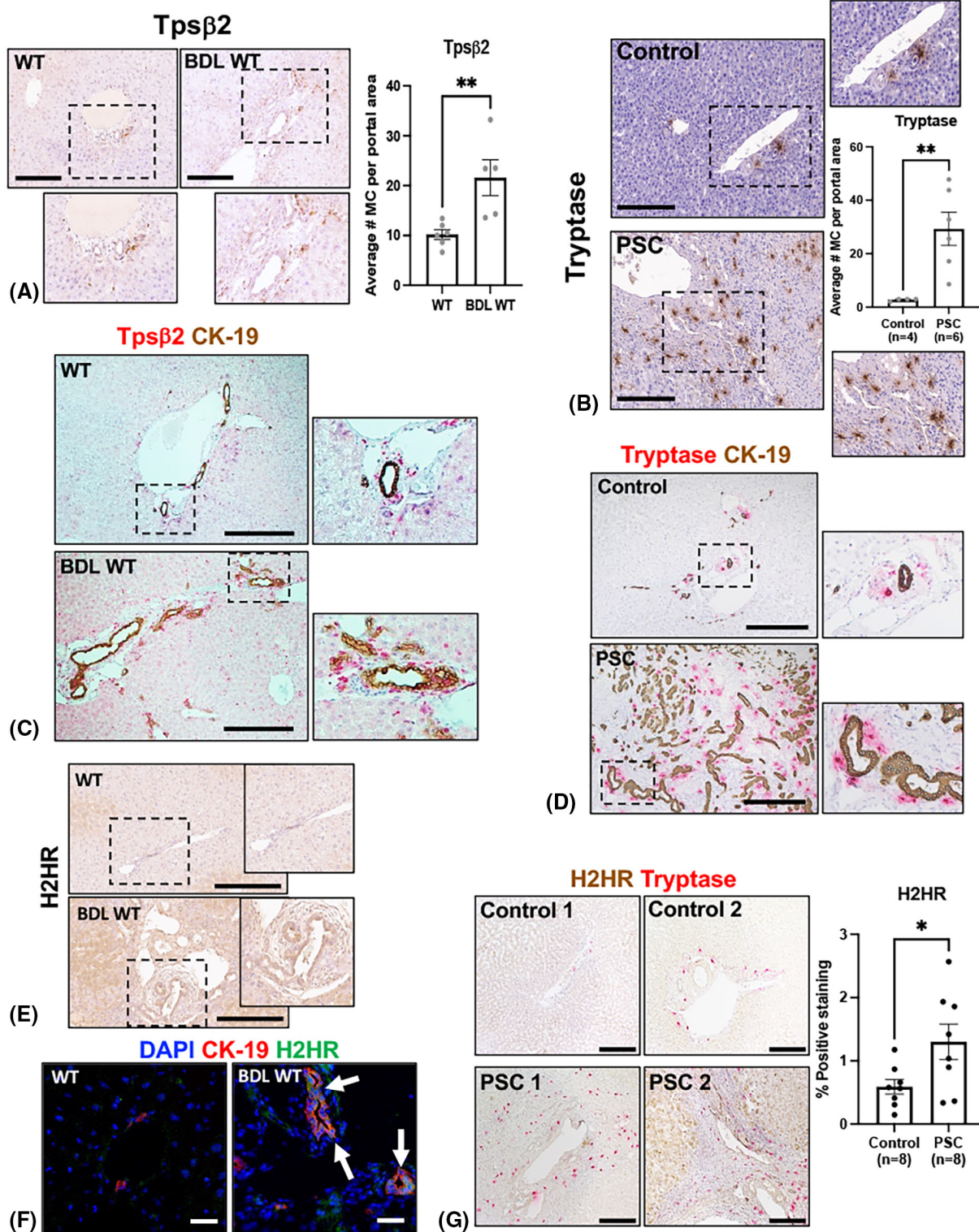
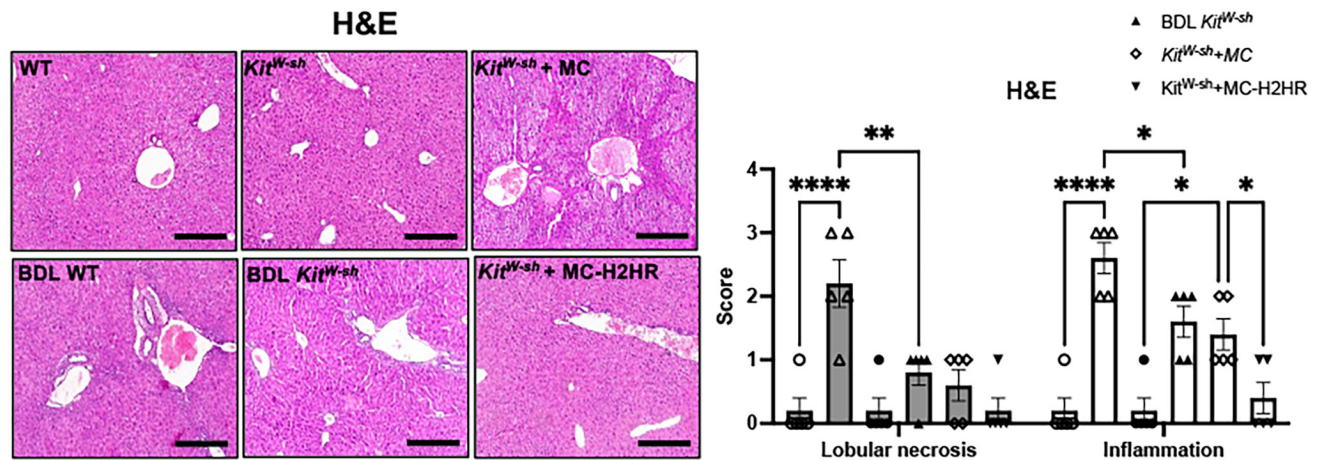
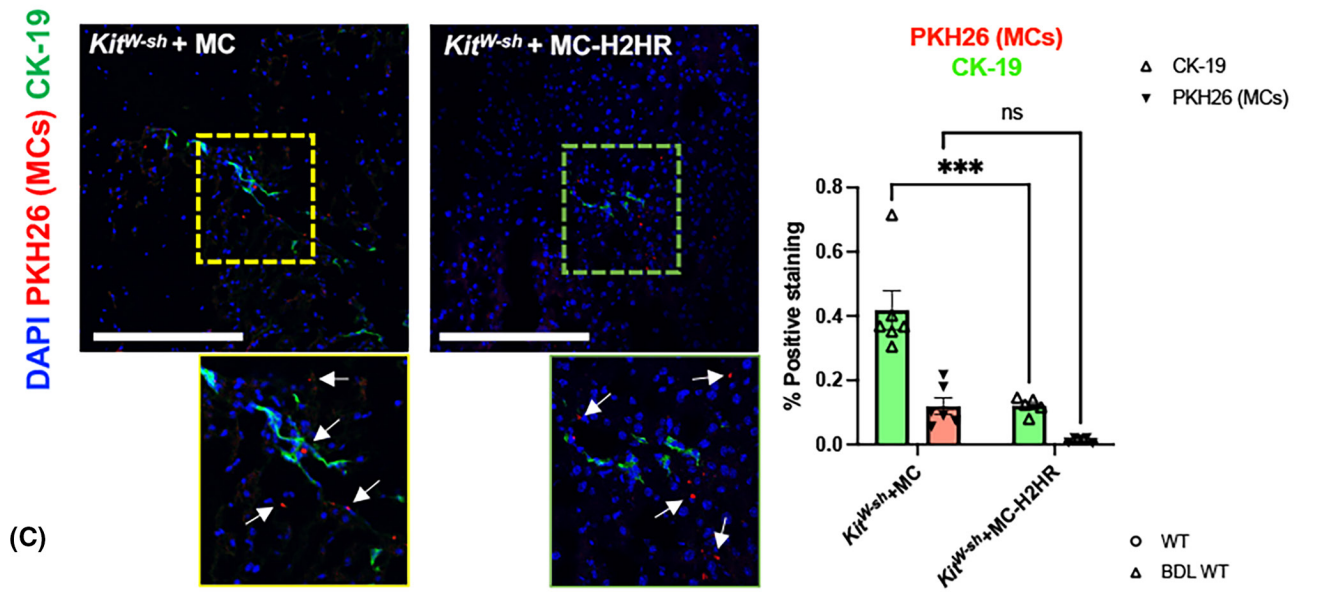
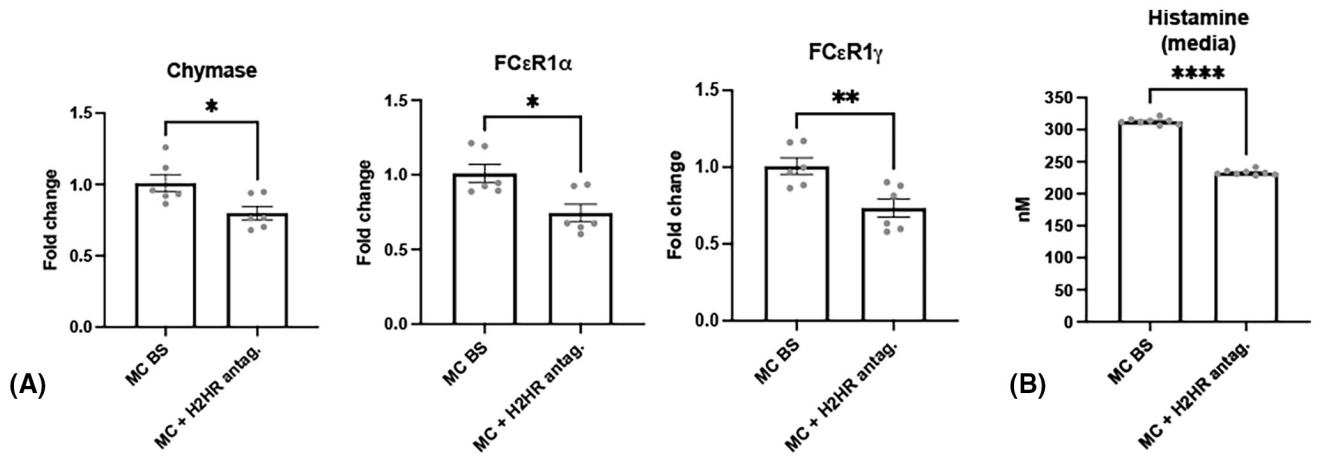


FIGURE 1 Evaluation of mast cell (MC) presence and biliary H2 histamine receptor (H2HR) expression. MC presence significantly increased in bile duct ligation (BDL) wild-type (WT) mice compared with WT mice (A) and in human primary sclerosing cholangitis (PSC) compared with controls (B). (C) There was increased tryptase beta 2 (Tps β 2)-positive MCs found close by large bile ducts (marked by cytokeratin 19 [CK-19]) in BDL WT mice. (D) In human PSC, tryptase (MC) and CK-19 positivity increased compared with control. MCs were found near bile ducts (inset image). By immunohistochemistry (E) and immunofluorescence (F), H2HR immunoreactivity increases in BDL WT compared with WT. H2HR expression was up-regulated primarily in large bile ducts (marked by white arrows) in BDL WT. (G) In PSC samples, H2HR immunoreactivity significantly increased in bile ducts compared with control samples, and MCs (tryptase) were found within the portal area. Data are presented as mean \pm SEM of $n = 3$ –5 portal tracts averaged per group from $n = 6$ mice/group, $n = 4$ control, and $n = 6$ PSC samples. * $p < 0.05$, ** $p < 0.01$. Representative images are shown at $\times 20$ and $\times 40$ for Tps β 2 and tryptase; $\times 10$ and $\times 40$ for Tps β 2/CK-19 and tryptase/CK-19; $\times 20$ and $\times 40$ for H2HR; $\times 40$ for H2HR/CK-19; and $\times 20$ for H2HR/tryptase. Scale bars are 200 μ m for Tps β 2, tryptase, Tps β 2/CK-19, tryptase/CK-19, and H2HR; and 100 μ m for H2HR/CK-19 and H2HR tryptase. Abbreviation: DAPI, 4',6-diamidino-2-phenylindole.



(D)

FIGURE 2 Validation of H2HR inhibition, MC injection model, and assessment of liver damage. In MCs treated with ranitidine (25 μ m, 48 h), chymase and FC epsilon receptor 1 subunits (FC ϵ R1 α and FC ϵ R1 γ) (A) and histamine (HA) secretion (B) decreased compared with basal treatments, confirming that inhibition of H2HR decreases MC activation. (C) Injected MCs were found in close proximity to bile ducts (white arrows), and semi-quantification was performed in two to three representative images ($\times 20$) per mouse ($n = 4-6$ mice/group), and dots represent the average positive area of one mouse. The number of CK-19-positive cholangiocytes decreased in *Kit*^{W-sh} mice injected with MC-H2HR; however, MC number was unchanged between groups. (D) In BDL WT, lobular necrosis and portal inflammation increased and was associated with large bile duct hyperplasia. BDL *Kit*^{W-sh} mice had significantly reduced portal inflammation and lobular necrosis. In *Kit*^{W-sh} mice injected with MCs, histology is mostly preserved; however, there is significantly increased portal inflammation compared to mice without MC injection that decreases in *Kit*^{W-sh} mice + MC-H2HR. Data are presented as mean \pm SEM of $n = 6$ experiments for quantitative polymerase chain reaction (PCR) and EIA. * $p < 0.05$, ** $p < 0.01$, **** $p < 0.0001$. Representative images are shown at $\times 40$ for immunofluorescence and $\times 10$ for hematoxylin and eosin (H&E). Inset image for immunofluorescence is $\times 80$. Scale bar for H&E = 300 μ m; scale bar for immunofluorescence = 50 μ m. Abbreviation: ns, not significant.

RESULTS

MC presence and biliary H2HR increase in BDL mice and patients with PSC

MC presence significantly increased within the portal tracts of BDL WT mice compared with WT (Figure 1A) and human PSC (Figure 1B) shown by immunostaining and semi-quantification. In BDL WT mice and patients with PSC, immunoreactivity of Tps β 2 and tryptase, respectively, increased, which was coupled with enhanced CK-19 positivity compared with controls (Figure 1C,D). In BDL WT mice, large-duct H2HR immunoreactivity increased compared with controls, as shown by immunohistochemistry and immunofluorescence (Figure 1E,F). Human PSC samples demonstrated significantly increased H2HR immunoreactivity in cholangiocytes along with elevated tryptase immunoreactivity compared with controls, signifying that MCs reside near H2HR-positive bile ducts (Figure 1G).

Inhibition of H2HR decreases MC activation *in vitro*, and injected MCs localize close by bile ducts *in vivo*

To validate that ranitidine inhibits MC activation before injection into *Kit*^{W-sh} mice, we found that chymase, FC ϵ R1 α , and FC ϵ R1 γ expression (Figure 2A) and HA secretion (Figure 2B) decreased in MCs treated with ranitidine compared with basal. Injected control or ranitidine-treated MCs (white arrows) were found surrounding bile ducts in *Kit*^{W-sh} mice (Figure 2C). Semi-quantification demonstrates that CK-19 positivity decreases in *Kit*^{W-sh} mice injected with MC-H2HR compared with control MC injections; however, the number of MCs found in the liver following TVI remains the same (Figure 2C). Together, these data validate that ranitidine decreases MC activation and that injected MCs localize to the liver close by bile ducts.

Hepatic damage, large IBDM, and biliary senescence decrease in *Kit*^{W-sh} mice injected with MC-H2HR

No significant histopathological features were present in WT and *Kit*^{W-sh} mice; however, BDL WT mice showed significantly increased lobular necrosis and portal inflammation associated with large bile duct hyperplasia (Figure 2D). BDL *Kit*^{W-sh} mice showed a significant reduction of portal inflammation and lobular necrosis along with decreased biliary hyperplasia. In *Kit*^{W-sh} mice injected with MCs, lobular necrosis remained similar, whereas inflammation was significantly increased compared to mice without MC injections, and this was significantly decreased in *Kit*^{W-sh} mice injected with MC-H2HR (Figure 2D).

BDL WT and *Kit*^{W-sh} mice injected with control MCs had increased large, but not small IBDM that was significantly reduced in BDL *Kit*^{W-sh} mice and *Kit*^{W-sh} mice injected with MC-H2HR (Figure 3A). Biliary senescence (indicated by p16 co-stained with CK-19) significantly increased in BDL-WT and *Kit*^{W-sh} mice injected with control MCs compared with controls (Figure 3B). When *Kit*^{W-sh} mice were injected with MC-H2HR, biliary senescence significantly decreased compared to *Kit*^{W-sh} mice injected with control MCs (Figure 3B). In human PSC samples, biliary p16 immunoreactivity and tryptase (MC) staining significantly increased compared with control (Figure 3C).

BDL *Kit*^{W-sh} and *Kit*^{W-sh} mice injected with MC-H2HR have decreased hepatic fibrosis, HSC activation, inflammation, and cAMP/ERK signaling compared with control injections

Hepatic fibrosis was significantly enhanced in BDL WT mice and in *Kit*^{W-sh} mice injected with control MCs compared with controls shown by FG/SR with semi-quantification (Figure 4A) and Masson's trichrome (Figure 4B). In BDL *Kit*^{W-sh} mice and *Kit*^{W-sh} mice injected

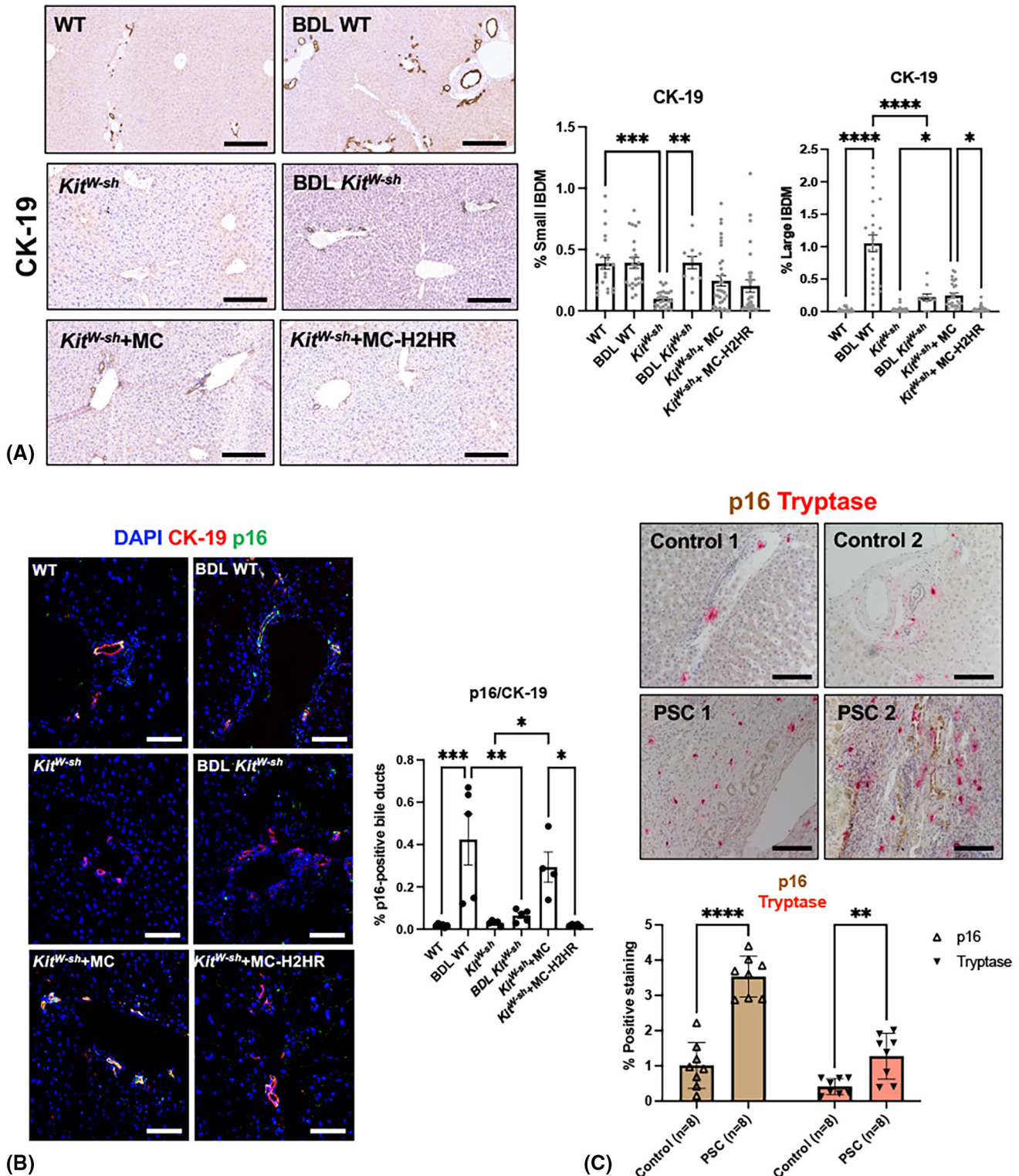


FIGURE 3 Determination of small and large intrahepatic bile duct mass (IBDM) and biliary senescence in mouse models along with MC/biliary senescence in human samples. (A) Bile duct ligation (BDL) WT mice have increased large, but not small, IBDM compared with WT. MC control injections increased large, but not small, IBDM, and in mice injected with MC-H2HR, large IBDM decreased. (B) Immunoreactivity for p16/CK-19 significantly increased in BDL WT and *Kit^{W-sh}* mice injected with control MCs compared with WT. In BDL *Kit^{W-sh}* mice and *Kit^{W-sh}* mice injected with MC-H2HR, p16 immunoreactivity significantly decreased compared with controls. (C) Primary sclerosing cholangitis (PSC) samples had significantly increased p16 immunoreactivity and MC presence compared with controls. Data are presented as mean \pm SEM of $n = 15$ –30 total images analyzed for CK-19 semi-quantification from $n = 6$ mice/group; each dot represents an image. Semi-quantification for p16/CK19 overlap area, as well as p16 and tryptase, were performed in two to three representative images ($\times 20$) per mouse ($n = 4$ –6 mice/group), and dots represent the average positive area of one mouse. * $p < 0.05$, ** $p < 0.01$, *** $p < 0.001$, **** $p < 0.0001$. Representative images are shown at $\times 10$ for CK-19; $\times 40$ for p16/CK-19; and $\times 20$ for p16/CK-19 immunostaining. Scale bar for CK-19 = 300 μm ; scale bar for immunofluorescence = 50 μm ; and scale bar for p16/CK-19 co-staining = 100 μm .

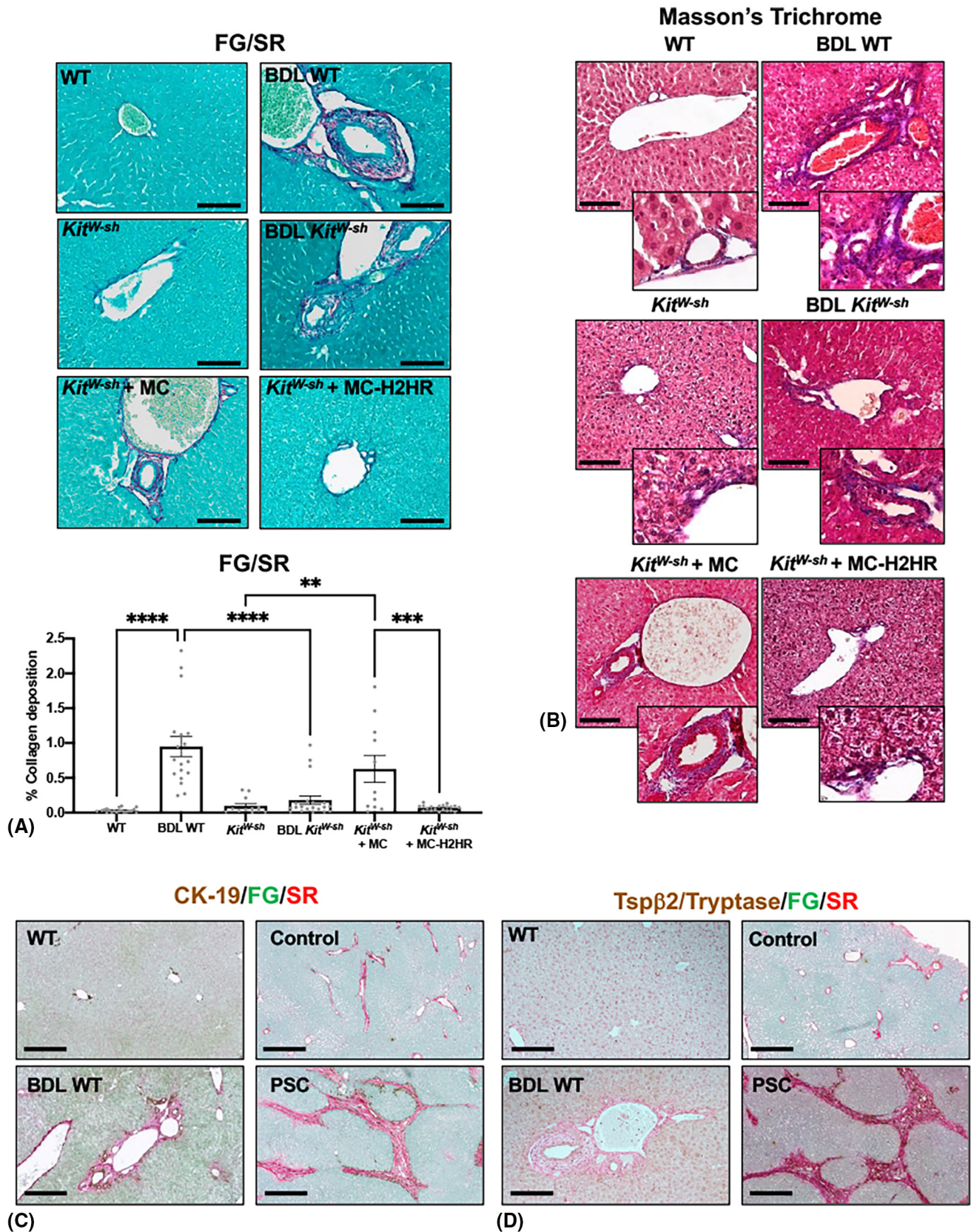


FIGURE 4 Legend on next page

with MC-H2HR, collagen deposition significantly reduced compared with control mice (Figure 4A,B). In BDL WT mice and PSC patient samples, collagen content (FG/SR)

increased around bile ducts (marked with CK-19) compared with controls (Figure 4C). Similarly, increased MC presence was found in fibrotic areas (marked by FG/SR)

FIGURE 4 Hepatic fibrosis and MC presence in animal models and human PSC. Collagen deposition, detected by fast green/sirius red (FG/SR) (with semi-quantification) (A) and Masson's trichrome (B), increased in BDL WT and *Kit^{W-sh}* mice injected with control MCs compared with WT, which was decreased in BDL *Kit^{W-sh}* mice or *Kit^{W-sh}* mice injected with MC-H2HR. (C) In BDL WT and human PSC there is increased collagen deposition surrounding bile ducts compared with WT. (D) In BDL WT and human PSC, MC presence increased, as shown by Tsp β 2 (mouse) and tryptase (human) alongside increased collagen deposition, compared with controls. Data are presented as mean \pm SEM of $n = 11$ – 20 total images analyzed for FG/SR semi-quantification from $n = 6$ mice/group; each dot represents an image. $**p < 0.01$, $***p < 0.001$, $****p < 0.0001$. Representative images are shown $\times 20$ for FG/SR and Masson's trichrome; $\times 10$ for FG/SR/CK-19; and $\times 10$ for FG/SR/Tsp β 2/tryptase. Scale bar for FG/SR and Masson's trichrome = $100\mu\text{m}$; scale bar for FG/SR/CK-19 and FG/SR/Tsp β 2/tryptase = $300\mu\text{m}$.

SR), as shown by Tsp β 2 in BDL WT mice and tryptase in human PSC (Figure 4D).

Immunoreactivity of desmin and GFAP significantly increased in BDL WT mice and *Kit^{W-sh}* mice injected with control MCs compared with controls, but was reduced in BDL *Kit^{W-sh}* mice and *Kit^{W-sh}* mice injected with MC-H2HR (Figure 5A,B).

Liver inflammation shown by F4/80 (Figure 5C) and CCL2 quantitative PCR (Figure 5D) significantly increased in BDL-WT mice and *Kit^{W-sh}* mice injected with control MCs; however, BDL *Kit^{W-sh}* mice and *Kit^{W-sh}* mice injected with MC-H2HR displayed significantly reduced liver inflammation.

cAMP immunoreactivity in bile ducts (white arrows) significantly increased in BDL WT mice and *Kit^{W-sh}* mice injected with control MCs compared with controls; however, this was reduced in BDL *Kit^{W-sh}* mice and *Kit^{W-sh}* mice injected with MC-H2HR (Figure 6A). Similarly, pERK immunoreactivity in bile ducts significantly increased in BDL WT compared with WT mice, and decreased in BDL *Kit^{W-sh}* compared with BDL WT mice (Figure 6B). Although not significant, there was a trend toward increased pERK immunoreactivity in bile ducts (white arrows) of *Kit^{W-sh}* mice injected with control MCs, which trended toward a decrease in *Kit^{W-sh}* mice injected with MC-H2HR (Figure 6B).

MCs preferentially migrate toward LMCCs, which are blocked by H2HR inhibition, *in vitro*

Before *in vitro* experiments, SMCCs and LMCCs were characterized for size and CK-19 expression. SMCCs

averaged $8.2\mu\text{m}$ and LMCC averaged $12.34\mu\text{m}$ in size when evaluated by trypan blue (Figure S1A). Both SMCCs and LMCCs were positive for CK-19, indicative of biliary origin (Figure S1B). At basal conditions, no significant changes in senescence were noted in SMCCs versus LMCCs; however, only LMCCs express H2HR (Figure S1B). MC migration increased only in LMCC treated with LPS compared with control, demonstrating MC preference to migrate toward injured large cholangiocytes (Figure S1C). In SMCCs and LMCCs treated with HA, MC migration increased compared with PBS treatments, presumably due to H1HR activity in SMCCs (Figure S2A); however, when LMCCs (but not SMCCs) were pretreated with the H2HR antagonist, MC migration was inhibited (Figure S2A,B), suggesting that the attraction between large cholangiocytes and MCs is mediated by H2HR signaling.

Inhibition of MC-derived HA decreases LMCC proliferation, senescence, H2HR, and cAMP/pERK, *in vitro*

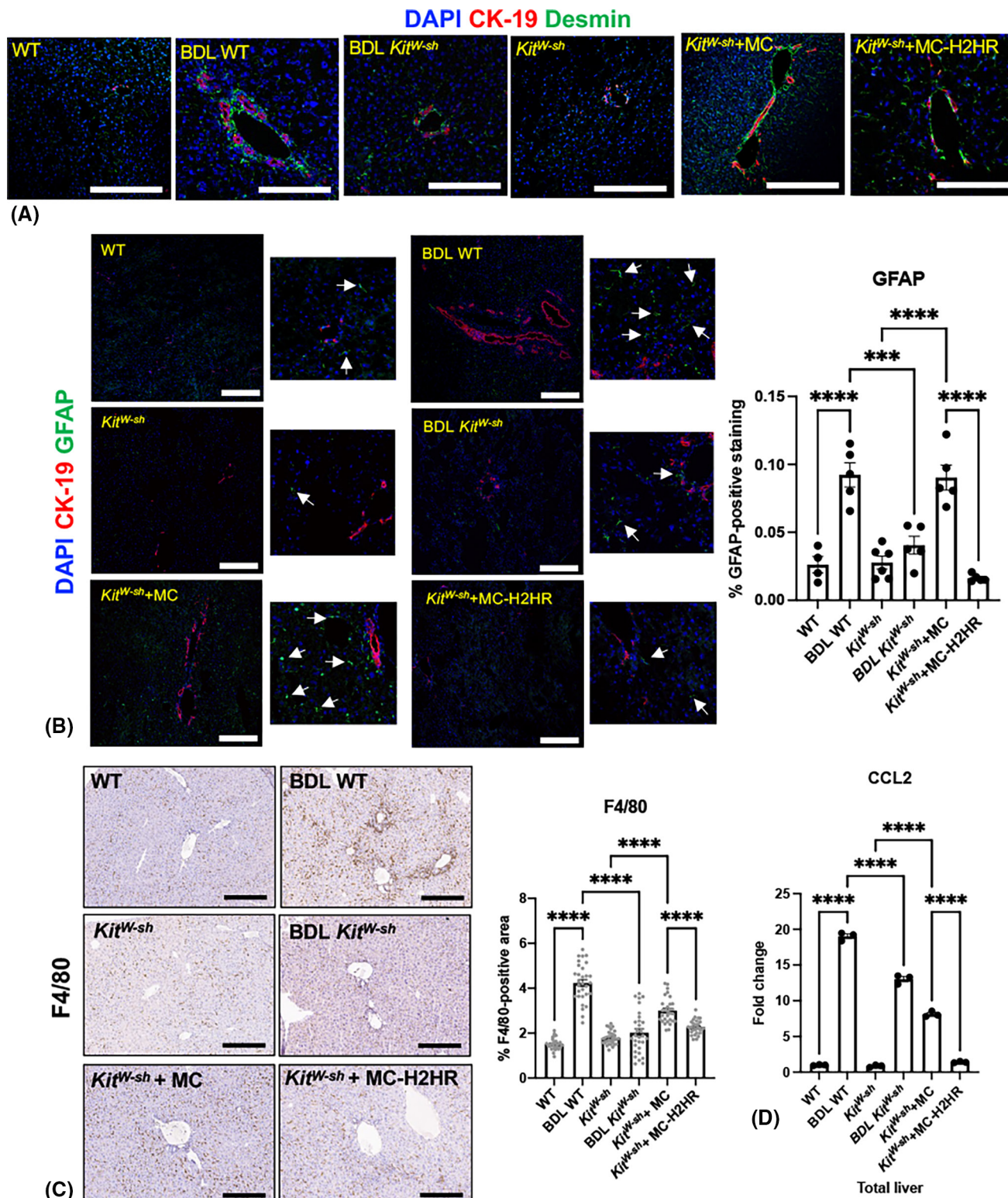
To demonstrate that MCs preferentially target large cholangiocytes, we found that LMCC, but not SMCC, senescence (p16 and p18 gene expression) increased after treatment with MC-conditioned media (Figure 7A). The immunoreactivity of p18 was unchanged in SMCCs treated with either basal or MCs; however, LMCCs treated with MCs had increased immunoreactivity of p18 compared with basal treatment (Figure 7B).

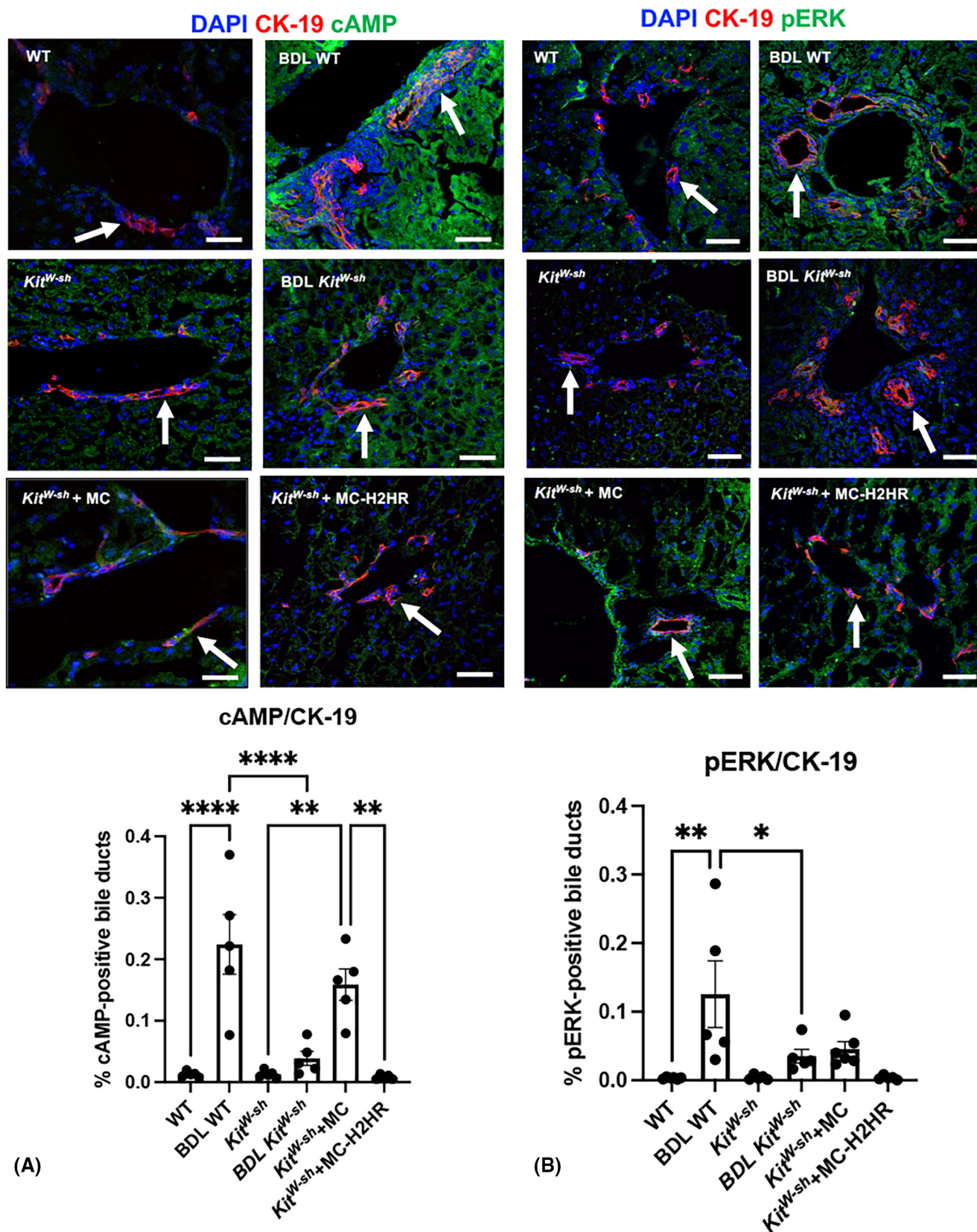
Next, we assessed the effect of blocking MC-derived HA on LMCC and demonstrated that LMCCs

FIGURE 5 HSC activation and inflammation in mouse models. (A) Desmin immunoreactivity increases in BDL WT and *Kit^{W-sh}* mice injected with control MCs compared with WT, which was reduced in BDL *Kit^{W-sh}* mice or *Kit^{W-sh}* mice injected with MC-H2HR compared with controls. (B) Glial fibrillary acidic protein (GFAP) immunoreactivity (white arrows) significantly increases in BDL WT and *Kit^{W-sh}* mice injected with control MCs compared with WT, which was reduced in BDL *Kit^{W-sh}* mice or *Kit^{W-sh}* mice injected with MC-H2HR compared with controls. (C) In BDL WT and *Kit^{W-sh}* mice injected with control MCs, F4/80-positive staining increases compared with WT, which reduces in both BDL *Kit^{W-sh}* mice or *Kit^{W-sh}* mice injected with MC-H2HR. (D) C-C motif chemokine ligand 2 (CCL2) expression increases in BDL WT and *Kit^{W-sh}* mice injected with control MCs compared with WT, which was reduced in BDL *Kit^{W-sh}* mice or *Kit^{W-sh}* mice injected with MC-H2HR compared with controls. Data are presented as mean \pm SEM of $n = 30$ total images analyzed for F4/80 semi-quantification from $n = 6$ mice/group; each dot represents an image. Semi-quantification for GFAP was performed in two to three representative images ($\times 20$) per mouse ($n = 4$ – 6 mice/group), and dots represent the average positive area of one mouse. Data are presented as mean \pm SEM of $n = 6$ experiments for quantitative PCR in total liver messenger RNA pooled from $n = 6$ mice per group. $***p < 0.001$, $****p < 0.0001$. Representative images are shown at $\times 20$ and $\times 80$ for immunofluorescence and $\times 10$ for F4/80. Scale bar for immunofluorescence = $250\mu\text{m}$; scale bar for F4/80 = $300\mu\text{m}$.

treated with MC-conditioned media had increased immunoreactivity p18, H2HR, and pERK compared with basal-treated LMCCs (Figure 7C). When MCs were pretreated with α -methyl (blocking HA synthesis), these parameters decreased, demonstrating that global inhibition of HA in MCs alters LMCC phenotypes

(Figure 7C). Next, we measured pERK phosphorylation by immunoblotting and found that MCs promote pERK phosphorylation (not significant), and when MCs are pretreated with α -methyl, there is a significant decrease in pERK phosphorylation (7D). Finally, we examined the effects of blocking MC-H2HR. We found that MC





media promotes LMCC senescence (p16 and p18), H2HR and pERK expression (Figure 7E), and cAMP levels (Figure 7F), which were decreased when MCs were pretreated with ranitidine.

DISCUSSION

In our study we demonstrate that MCs preferentially interact with large, senescent cholangiocytes during

FIGURE 6 Extracellular signal-regulated protein kinase (pERK)/cyclic adenosine monophosphate (cAMP) immunoreactivity in mouse models. (A) cAMP in bile ducts (white arrows) increased in BDL WT and *Kit^{W-sh}* mice injected with control MCs compared with controls; however, this significantly decreased in BDL *Kit^{W-sh}* mice and *Kit^{W-sh}* mice injected with MC-H2HR. (B) pERK expression in bile ducts (white arrows) significantly increased in BDL WT compared with WT mice, and significantly decreased in BDL *Kit^{W-sh}* mice compared with BDL WT. pERK immunoreactivity trended toward an increase in *Kit^{W-sh}* mice injected with control MCs and trended toward a decrease in *Kit^{W-sh}* mice injected with MC-H2HR. Data are presented as mean \pm SEM. Semi-quantification for cAMP/CK-19 and pERK/CK-19 was performed in two to three representative images ($\times 20$) per mouse ($n = 4-6$ mice/group), and dots represent the average positive area of one mouse. * $p < 0.05$, ** $p < 0.01$, **** $p < 0.0001$. Representative images are shown at $\times 40$ for cAMP/CK-19 and pERK/CK-19 immunofluorescence. Scale bar for cAMP/CK-19 and pERK/CK-19 = 50 μm .

biliary damage, including cholestatic and MC-induced injury via H2HR signaling. In both animal models and human PSC, MCs are found near large, senescent bile ducts that express increased levels of H2HR. In MC-deficient mice injected with H2HR-inhibited MCs, we found reduced large IBDM, hepatic fibrosis, biliary senescence, and inflammation.

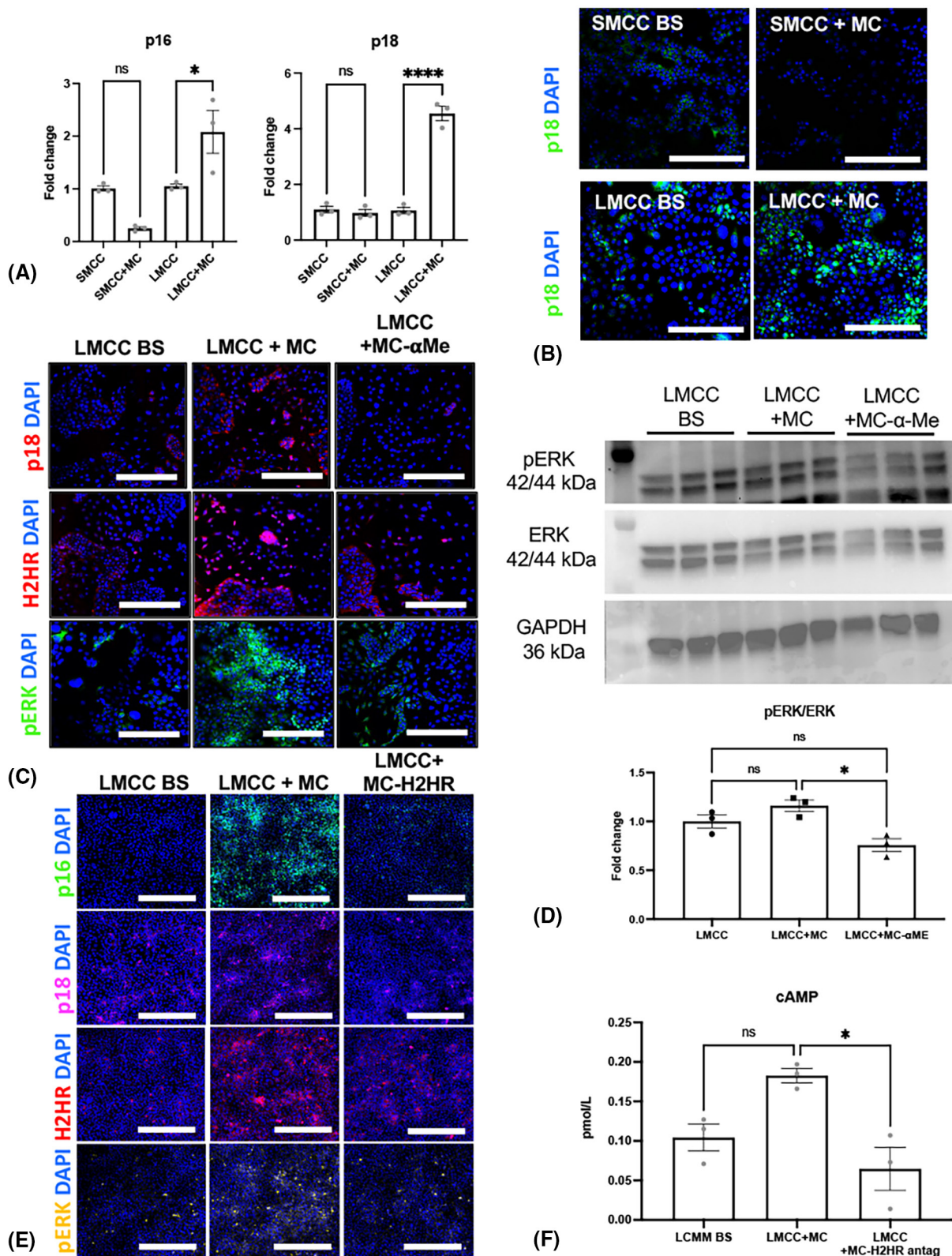
Cholangiopathies occur in specific portions of the biliary tree and explicitly target certain segments of the biliary epithelium. For example, patients with PSC may present with (i) classic PSC that targets large bile ducts, (ii) small-duct PSC, or (iii) PSC associated with autoimmune hepatitis, which affects both small and large bile ducts.^[20] Typically, large-duct PSC increases CCA risk; however, patients may be encumbered with tumors of the intrahepatic or extrahepatic bile duct.^[21] More commonly, Klatskin tumors are hilar in location and demonstrate the extrahepatic manifestation of CCA associated with PSC.^[22] In animal models of cholestatic liver injury and nonalcoholic fatty liver disease (NAFLD), as well as in human patients (e.g., PSC, NAFLD, nonalcoholic steatohepatitis [NASH]), MCs are adjacent to portal tracts.^[23] Similar to our present study, MC presence corresponds with increasing IBDM,^[16] and increased MC infiltration directly correlates with enhanced fibrosis in patients with PBC and alcohol-induced liver injury.^[24] In patients with biliary atresia, MCs positively correlate with enhanced fibrosis and increased interleukin (IL)-33 signaling; worsening prognosis was also associated with increased MC presence.^[25] In patients with stage 3-4 NASH, hepatic fibrosis correlated with MC number, which was increased compared with controls.^[26]

We found that MCs migrated to large, senescent bile ducts in rodent models, and in patients with PSC, MCs were found near p16-positive bile ducts, suggesting that senescent cholangiocytes attract MCs. Supporting this, inhibition of SCF using Vivo Morpholino decreased PSC phenotypes and MC infiltration in *Mdr2^{-/-}* mice, suggesting that SCF (secreted by mouse and human cholangiocytes) attracts KIT-positive MCs to the portal tract.^[17] Biliary senescence affects cholestatic liver injury^[27]; however, the link between senescent cholangiocytes and MC infiltration remains elusive. CCL-5 is a SASP factor implicated in clear cell renal cell carcinoma (ccRCC) tumor progression, and MC migration was dependent on CCL-5 in human ccRCC and increased CCL-5 expression,

and MC presence correlated with poor prognosis.^[28] We found that blocking MC-H2HR before injection decreased biliary senescence, indicating that manipulation of MC components directly regulates this phenotype.

Hepatic fibrosis and inflammation are major features of PSC and may be consequences of increased DR. Additionally, in BDL *Kit^{W-sh}* mice and western diet-fed *Kit^{W-sh}* mice, hepatic fibrosis and inflammation are markedly reduced compared with controls.^[15,23] Furthermore, an injection of mouse MCs in *Kit^{W-sh}* mice^[15] promotes hepatic fibrosis and inflammation, suggesting that MCs play a key role in these processes. Using a double knockout mouse model lacking HA created by crossing *Mdr2^{-/-}* mice with *HDC^{-/-}* mice, we demonstrated that blocking the HDC/HA axis in *Mdr2^{-/-}* mice ameliorates PSC phenotypes, and when these mice were injected with mouse MCs, hepatic fibrosis and inflammation increased.^[29] In the present study, large IBDM was associated with enhanced hepatic fibrosis in *Mdr2^{-/-}* mice and human PSC, and when MC-H2HR was inhibited, fibrosis decreased. MC injection into WT or *Kit^{W-sh}* mice induces cholestatic-like liver injury^[18,30] and exacerbates liver damage in western diet-fed mice^[23] by promoting DR and biliary senescence. Before injection, inhibition of MC-transforming growth factor- β signaling or farnesoid X receptor activity reduces MC-induced features of cholestatic damage,^[18,30] suggesting that manipulation of MC components is a targetable maneuver to ameliorate injury.

Small cholangiocytes signal primarily through Ca^{2+} -dependent mechanisms, whereas large cholangiocytes are preferential to cAMP signaling and downstream mediators like ERK1/2.^[5,6] Furthermore, small H1HR-positive cholangiocytes are regulated by Ca^{2+} signaling and large H2HR-positive cholangiocytes via cAMP.^[12] In this study, we surmised that the effects of inhibition of MC-H2HR might be regulated by biliary cAMP/ERK1/2. When mice were injected with control MCs, cAMP/pERK expression increased, which decreased in MC-H2HR-injected mice. Furthermore, we found that *Mdr2/HDC* double-knockout mice have decreased H2HR and pERK signaling that were restored when *Mdr2/HDC* mice were injected with exogenous HA.^[29] Although we have shown that inhibition of H2HR reduces large IBDM



and cAMP/pERK signaling,^[19] our present study demonstrates the paracrine crosstalk between MC-H2HR and biliary cAMP/pERK intracellular signaling. We further validated this in our *in vitro* experiments, which demonstrate that when MCs are co-cultured with LMCCs, cAMP/pERK expression increases,

which was blocked when MCs were pretreated with α -Me. To support our findings, *in vitro*, human MCs were found to express H4HR and secrete IL-1 β , which caused activation of stress-activated protein kinases (SAPK)/jun amino-terminal kinases (JNK) signaling pathways, and when H4HR was silenced with small

FIGURE 7 *In vitro*, impact of MC-derived HA and MC-H2HR on large cholangiocyte phenotypes. (A) Treatment with MC-conditioned media increased p16 and p18 expression in large mouse cholangiocytes (LMCCs), but not small mouse cholangiocytes (SMCCs), as shown by quantitative PCR. (B) p18 immunoreactivity increased in LMCCs (but not SMCCs) treated with MC-conditioned media compared with basal treatments. (C) *In vitro* treatment with MC-conditioned media increased p18, H2HR, and pERK immunoreactivity in LMCCs compared with basal-treated LMCCs, which was reduced when MCs were pretreated α -methyl. (D) Immunoblotting revealed that LMCCs treated with MC-conditioned media had a tendency to increase ERK phosphorylation (pERK); however, when LMCCs were pretreated with ranitidine, ERK phosphorylation significantly decreased compared with control. (E) LMCCs treated with MC-conditioned media confirmed increased senescence (p16 and p18), H2HR, and pERK expression compared with basal-treated LMCCs; however, when MCs were pretreated with α -methyl, these phenotypes decreased. (F) cAMP activity in LMCCs enhanced following treatment with MC-conditioned media but reduced in LMCCs treated with media from MCs pretreated with ranitidine. Data are presented as mean \pm SEM of $n = 3$ experiments for enzyme-linked immunosorbent assay (ELISA) and immunoblots. * $p < 0.05$, **** $p < 0.0001$. Representative images are shown at $\times 20$. Scale bar for immunofluorescence = $250 \mu\text{m}$. Representative bands are shown for pERK, total extracellular signal-regulated kinase (ERK), and glyceraldehyde 3-phosphate dehydrogenase (GAPDH).

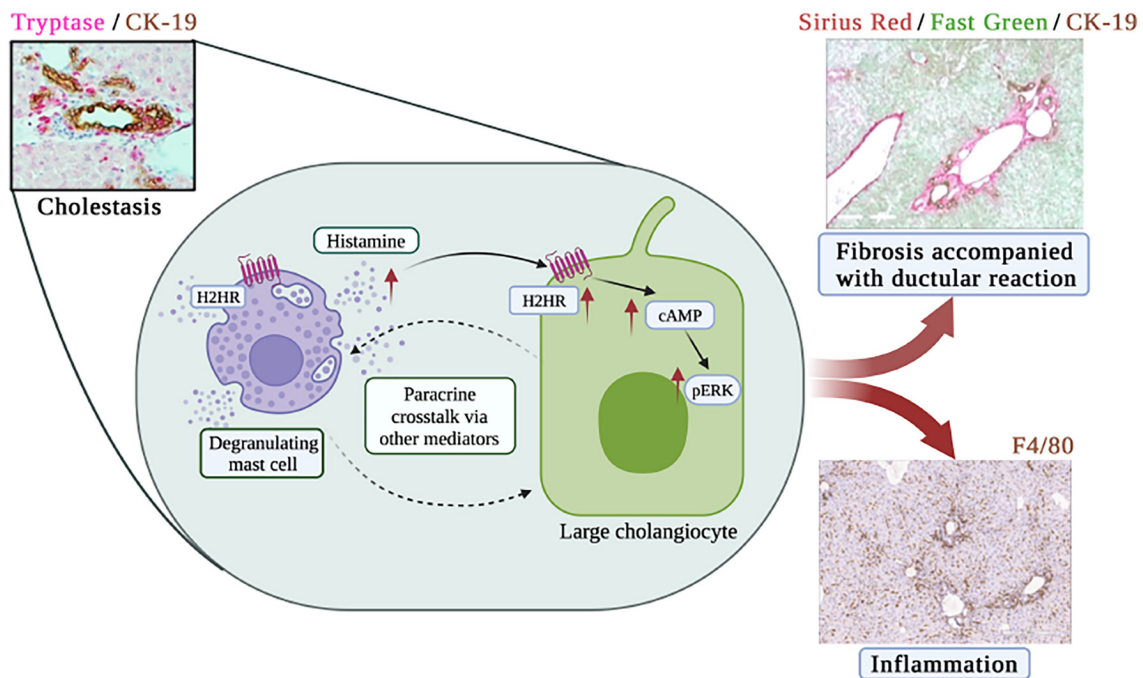


FIGURE 8 Working model. During liver injury, paracrine crosstalk between cholangiocytes and MCs is regulated by MC-H2HR, which promotes cholestatic phenotypes. There is an association between MCs and large IBDM and senescence, suggesting that MCs preferentially interact with large cholangiocytes during damage. Moreover, large cholangiocyte–MC crosstalk influences inflammation and portal/peribiliary fibrosis. Inhibition of MC-H2HR ameliorates cholestatic damage by decreasing ductular reaction, biliary senescence, hepatic fibrosis, and inflammation.

interfering RNA, MC-dependent IL-1 β and SAPK/JNK signaling was reduced.^[31]

MC-H2HR signaling contributes to MC chemotaxis, and inhibition of large cholangiocyte H2HR blocked MC migration, demonstrating the interaction between cholangiocytes and MCs via H2HR. In our study we find an increase in biliary H2HR in both mouse models and human PSC; however, our analysis could not rule out the potential contribution of other liver cells such as hepatocytes or Kupffer cells. Furthermore, MCs themselves also express H2HR, thus inducing a paracrine interaction between cholangiocytes and MCs during liver injury. Previous work found that H4HR signaling induces chemotaxis of MCs into the lung, and when H4HR was inhibited, MC accumulation decreased.^[32] The authors also

found that H1HR and H4HR expression increased in lung; however, manipulation of H1HR did not alter MC accumulation.^[32] In melanoma tumorigenesis, MC infiltration promotes angiogenesis and hypoxia-inducible factor (HIF-1 α) production, and inhibition of H1HR decreased MC accumulation in tumors along with reduced angiogenesis and HIF-1 α expression,^[33] supporting the concept that MC-H2HR manipulation alters MC accumulation and pathological effects.

In summary, we demonstrated that paracrine crosstalk between large cholangiocytes and MCs is regulated by H2HR, which promotes cholestatic phenotypes (Figure 8). There is an association between MCs and large IBDM and senescence, suggesting that MCs preferentially interact with large

cholangiocytes during damage. Moreover, large cholangiocyte–MC crosstalk influences inflammation and portal/peribiliary fibrosis, preferentially around large ducts. Inhibition of MC-H2HR ameliorates cholestatic damage by decreasing DR, biliary senescence, hepatic fibrosis, and inflammation. Further studies are warranted to fully understand the role of MC HR signaling during liver disease.

ACKNOWLEDGMENT

We acknowledge and thank Corinn Marakovits for her assistance with quantification of immunofluorescent and immunohistochemical staining.

FUNDING INFORMATION

Supported by the Hickam Endowed Chair, Gastroenterology, Medicine (Indiana University), the Indiana University Health–Indiana University School of Medicine Strategic Research Initiative, the Senior Career Scientist Award (IK6 BX004601), and the VA Merit award (5I01BX000574) to G.A.; the Career Scientist Award (IK6BX005226) and the VA Merit award (1I01BX003031) to H.F.; the Career Development Award-2 (1IK2BX005306) from the United States Department of Veterans Affairs to L.K.; Biomedical Laboratory Research and Development Service and National Institutes of Health grants (DK108959, DK119421, DK054811, DK115184, DK076898, DK107310, DK110035, DK062975, and AA028711); and PSC Partners Seeking a Cure. Portions of these studies were supported by resources at the Richard L. Roudebush VA Medical Center (Indianapolis, Indiana) and Medical Physiology (Temple, Texas).

CONFLICT OF INTEREST

Nothing to report.

DISCLOSURES

This material is the result of work supported by resources at the Richard L. Roudebush VA Medical Center. The content is the responsibility of the author(s) alone and does not necessarily reflect the views or policies of the Department of Veterans Affairs or the United States Government.

ORCID

Guido Carpino  <https://orcid.org/0000-0001-8570-2519>

Burcin Ekser  <https://orcid.org/0000-0003-0741-8007>

Gianfranco Alpini  <https://orcid.org/0000-0002-6658-3021>

Lindsey Kennedy  <https://orcid.org/0000-0001-9224-8940>

Lindsey Kennedy  <https://orcid.org/0000-0001-9224-8940>

Heather Francis  <https://orcid.org/0000-0002-3466-3545>

Heather Francis  <https://orcid.org/0000-0002-3466-3545>

REFERENCES

- Alpini G, Roberts S, Kuntz SM, Ueno Y, Gubba S, Podila PV, et al. Morphological, molecular, and functional heterogeneity

- of cholangiocytes from normal rat liver. *Gastroenterology*. 1996;110:1636–43.
- Benedetti A, Bassotti C, Rapino K, Marucci L, Jezequel AM. A morphometric study of the epithelium lining the rat intrahepatic biliary tree. *J Hepatol*. 1996;24:335–42.
- Glaser SS, Gaudio E, Rao A, Pierce LM, Onori P, Franchitto A, et al. Morphological and functional heterogeneity of the mouse intrahepatic biliary epithelium. *Lab Invest*. 2009;89:456–69.
- Glaser S, Francis H, Demorrow S, Lesage G, Fava G, Marzioni M, et al. Heterogeneity of the intrahepatic biliary epithelium. *World J Gastroenterol*. 2006;12:3523–36.
- Francis H, Franchitto A, Ueno Y, Glaser S, DeMorrow S, Venter J, et al. H3 histamine receptor agonist inhibits biliary growth of BDL rats by downregulation of the cAMP-dependent PKA/ERK1/2/ELK-1 pathway. *Lab Invest*. 2007;87:473–87.
- Francis H, Glaser S, Demorrow S, Gaudio E, Ueno Y, Venter J, et al. Small mouse cholangiocytes proliferate in response to H1 histamine receptor stimulation by activation of the IP3/CaMK I/CREB pathway. *Am J Physiol Cell Physiol*. 2008;295:C499–513.
- LeSage GD, Benedetti A, Glaser S, Marucci L, Tretjak Z, Caligiuri A, et al. Acute carbon tetrachloride feeding selectively damages large, but not small, cholangiocytes from normal rat liver. *Hepatology*. 1999;29:307–19.
- LeSage GD, Glaser SS, Marucci L, Benedetti A, Phinizz JL, Rodgers R, et al. Acute carbon tetrachloride feeding induces damage of large but not small cholangiocytes from BDL rat liver. *Am J Physiol*. 1999;276:G1289–301.
- Mancinelli R, Franchitto A, Glaser S, Meng F, Onori P, DeMorrow S, et al. GABA induces the differentiation of small into large cholangiocytes by activation of Ca(2+) /CaMK I-dependent adenylyl cyclase 8. *Hepatology*. 2013;58:251–63.
- Kennedy L, Hargrove L, Demieville J, Francis N, Seils R, Villamaria S, et al. Recent advances in understanding cholangiocarcinoma. *F1000Res*. 2017;6:1818.
- Francis H, Meng F, Gaudio E, Alpini G. Histamine regulation of biliary proliferation. *J Hepatol*. 2012;56:1204–6.
- Francis HL, Demorrow S, Franchitto A, Venter JK, Mancinelli RA, White MA, et al. Histamine stimulates the proliferation of small and large cholangiocytes by activation of both IP3/Ca2+ and cAMP-dependent signaling mechanisms. *Lab Invest*. 2012;92:282–94.
- Jarido V, Kennedy L, Hargrove L, Demieville J, Thomson J, Stephenson K, et al. The emerging role of mast cells in liver disease. *Am J Physiol Gastrointest Liver Physiol*. 2017;313:G89–G101.
- Kennedy L, Hargrove L, Demieville J, Karstens W, Jones H, DeMorrow S, et al. Blocking H1/H2 histamine receptors inhibits damage/fibrosis in Mdr2(–/–) mice and human cholangiocarcinoma tumorigenesis. *Hepatology*. 2018;68:1042–56.
- Hargrove L, Kennedy L, Demieville J, Jones H, Meng F, DeMorrow S, et al. Bile duct ligation-induced biliary hyperplasia, hepatic injury, and fibrosis are reduced in mast cell-deficient Kit(W-sh) mice. *Hepatology*. 2017;65:1991–2004.
- Kennedy LL, Hargrove LA, Graf AB, Francis TC, Hodges KM, Nguyen QP, et al. Inhibition of mast cell-derived histamine secretion by cromolyn sodium treatment decreases biliary hyperplasia in cholestatic rodents. *Lab Invest*. 2014;94:1406–18.
- Meadows V, Kennedy L, Hargrove L, Demieville J, Meng F, Virani S, et al. Downregulation of hepatic stem cell factor by Vivo-Morpholino treatment inhibits mast cell migration and decreases biliary damage/senescence and liver fibrosis in Mdr2(–/–) mice. *Biochim Biophys Acta Mol Basis Dis*. 2019;1865:165557.
- Kyritsi K, Kennedy L, Meadows V, Hargrove L, Demieville J, Pham L, et al. Mast cells (MCs) induce ductular reaction mimicking liver injury in mice via MC-derived TGF-beta1 signaling. *Hepatology*. 2021;73:2397–410.
- Kennedy L, Meadows V, Demieville J, Hargrove L, Virani S, Glaser S, et al. Biliary damage and liver fibrosis are ameliorated

- in a novel mouse model lacking l-histidine decarboxylase/histamine signaling. *Lab Invest.* 2020;100:837–48.
20. Saich R, Chapman R. Primary sclerosing cholangitis, autoimmune hepatitis and overlap syndromes in inflammatory bowel disease. *World J Gastroenterol.* 2008;14:331–7.
 21. Blechacz B, Gores GJ. Cholangiocarcinoma: advances in pathogenesis, diagnosis, and treatment. *Hepatology.* 2008;48:308–21.
 22. Bridgewater J, Galle PR, Khan SA, Llovet JM, Park JW, Patel T, et al. Guidelines for the diagnosis and management of intrahepatic cholangiocarcinoma. *J Hepatol.* 2014;60:1268–89.
 23. Kennedy L, Meadows V, Sybenga A, Demieville J, Chen L, Hargrove L, et al. Mast cells promote nonalcoholic fatty liver disease phenotypes and microvesicular steatosis in mice fed a western diet. *Hepatology.* 2021;74:164–82.
 24. Farrell DJ, Hines JE, Walls AF, Kelly PJ, Bennett MK, Burt AD. Intrahepatic mast cells in chronic liver diseases. *Hepatology.* 1995;22(4 Pt 1):1175–81.
 25. Liu J, Yang Y, Zheng C, Chen G, Shen Z, Zheng S, et al. Correlation of interleukin-33/ST2 receptor and liver fibrosis progression in biliary atresia patients. *Front Pediatr.* 2019;7:403.
 26. Stal P. Liver fibrosis in non-alcoholic fatty liver disease—diagnostic challenge with prognostic significance. *World J Gastroenterol.* 2015;21:11077–87.
 27. Nakanuma Y, Sasaki M, Harada K. Autophagy and senescence in fibrosing cholangiopathies. *J Hepatol.* 2015;62:934–45.
 28. Liu T, Xia Q, Zhang H, Wang Z, Yang W, Gu X, et al. CCL5-dependent mast cell infiltration into the tumor microenvironment in clear cell renal cell carcinoma patients. *Aging (Albany NY).* 2020;12:21809–36.
 29. Kennedy L, Meadows V, Kyritsi K, Pham L, Kundu D, Kulkarni R, et al. Alemiroation of large bile duct damage by histamine-2 receptor vivo-morpholino treatment. *Am J Pathol.* 2020;190:1018–29.
 30. Meadows V, Kennedy L, Ekser B, Kyritsi K, Kundu D, Zhou T, et al. Mast cells regulate ductular reaction and intestinal inflammation in cholestasis via farnesoid X receptor signaling. *Hepatology.* 2021;74:2684–98.
 31. Ebenezer AJ, Prasad K, Rajan S, Thangam EB. Silencing of H4R inhibits the production of IL-1beta through SAPK/JNK signaling in human mast cells. *J Recept Signal Transduct Res.* 2018;38:204–12.
 32. Kay LJ, Suvarna SK, Peachell PT. Histamine H4 receptor mediates chemotaxis of human lung mast cells. *Eur J Pharmacol.* 2018;837:38–44.
 33. Jeong HJ, Oh HA, Nam SY, Han NR, Kim YS, Kim JH, et al. The critical role of mast cell-derived hypoxia-inducible factor-1alpha in human and mice melanoma growth. *Int J Cancer.* 2013;132:2492–501.

SUPPORTING INFORMATION

Additional supporting information can be found online in the Supporting Information section at the end of this article.

How to cite this article: Zhou T, Meadows V, Kundu D, Kyritsi K, Owen T, Ceci L, Mast cells selectively target large cholangiocytes during biliary injury via H2HR-mediated cAMP/pERK1/2 signaling. *Hepatol Commun.* 2022;6:2715–2731. <https://doi.org/10.1002/hep4.2026>